GEOPHYSICAL RESEARCH LETTERS, VOL. 25, NO. 11, PAGES 1833-1836, JUNE 1, 1998

A saturation mechanism for the Farley-Buneman instability

Niels F. Otani[1]

Department of Physics and Astronomy, University of Iowa, Iowa City, Iowa

Meers Oppenheim

Physics Department, University of Colorado, Boulder, Colorado

Abstract. Studies with a reduced-mode two-fluid model have revealed a promising candidate for the saturation mechanism of the Farley-Buneman instability in the daytime equatorial electrojet. The mechanism operates by redistributing the zero-order electron $\mathbf{E} \times \mathbf{B}$ flow field. Secondary waves generated nonlinearly by the instability are responsible for the flow field modification. Saturation occurs because the modified flow reduces the principal charge transport responsible for the growth of the primary wave. Two-dimensional particle simulations of the instability exhibit saturation via the same mechanism.

Introduction

Type-1 radar echoes indicate the presence of naturally occurring plasma waves in the Earth's equatorial and auroral electrojets. The linear theory of the Farley-Buneman instability effectively explains many of the observed behaviors of type-1 radar echoes including the conditions necessary for the onset of these waves, the wave propagation direction and, roughly, their dominant wavelengths. However, this theory fails to explain a number of other observations, notably the phase velocity measured by radar, the spectral shape and the saturated wave amplitude [*Buneman*, 1963; *Farley*, 1963]. To explain these features, one must understand the behavior of nonlinearly saturated Farley-Buneman waves, a subject studied for thirty years [*Sudan et al.*, 1973; *Sudan*, 1983; *Hamza and St-Maurice*, 1993; *Sahr and Farley*, 1995]. In this Letter, we describe a new saturation mechanism for the Farley-Buneman instability found in the course of studying a reduced-mode two-fluid computer model. We believe this mechanism may cause saturation of type-1 waves in the daytime equatorial electrojet, because it operates both in our reduced mode model and in full 2D particle simulations of the instability.

The reduced mode model simplifies the task of understanding the behavior of Farley-Buneman instability, but does not represent its full nonlinear and kinetic behavior. Fortunately, the saturation mechanism identified in the reduced mode model also appears to dominate the behavior of kinetic particle simulations, which, in turn, exhibit many of the observed characteristics of type-1 irregularities not explained by linear theory [*Oppenheim et al.*, 1995, 1996; *Oppenheim and Otani*, 1996]. Both models point to the nonlinear electron $\mathbf{E} \times \mathbf{B}$ drift term as the dominant nonlinear term and, further, show the appearance of vertically propagating secondary waves as the horizontally traveling primary Farley-Buneman wave saturates. On the basis of these facts, we believe it is likely that (1) mode coupling is responsible for the appearance of the secondary waves, (2) secondary waves are responsible for the saturation of the Farley-Buneman instability in the simulations through the mechanism outlined in this letter, and (3) the saturation mechanism operating in the simulation is also acting to saturate the Farley-Buneman instability in the daytime equatorial electrojet.

The Mode-Coupling Model

The reduced mode-coupling model used for this study represents the ions as a warm, unmagnetized fluid damped through ion-neutral collisions. The linearized ion continuity and momentum equations for the spatial Fourier component corresponding to wavevector $\mathbf{k}$ may be written as,

$$(\partial_t + i\mathbf{k}\cdot\mathbf{u}_{i0})n_{\mathbf{k}} = -n_0 i\mathbf{k}\cdot\mathbf{u}_{i\mathbf{k}}, \tag{1}$$

and,

$$(\partial_t + i\mathbf{k}\cdot\mathbf{u}_{i0} + \nu_i)\mathbf{u}_{i\mathbf{k}} = -\frac{e}{m_i} i\mathbf{k}\phi_{\mathbf{k}} - \frac{\gamma_i T_i}{m_i n_0} i\mathbf{k} n_{\mathbf{k}}. \tag{2}$$

where $\mathbf{u}_{i0}$ is the (generally small) zero-order ion Pedersen drift. The electrons in the model obey a mobility equation of the form, $\mathbf{u}_e = \mu_e \cdot \mathbf{E}$, in the plane perpendicular to the Earth's magnetic field $\mathbf{B}_0$, with μ_e being a tensor involving the standard electron Pedersen and Hall mobilities. Substituting into the quasineutrality condition, $\nabla \cdot \mathbf{J} = 0$, (with $n_e \approx n_i$), we obtain,

$$-\frac{e}{m_i} n_0 k^2 \phi_{\mathbf{k}} + \left(\frac{\gamma_e T_e}{m_i} k^2 + \bar{\nu} i\mathbf{k}\cdot(\mathbf{V}_{de0} - \mathbf{u}_{i0})\right) n_{\mathbf{k}}$$
$$-\bar{\nu} n_0 i\mathbf{k}\cdot\mathbf{u}_{i\mathbf{k}} = \frac{e}{m_i}\frac{|\Omega_e|}{\nu_e} \sum_{\mathbf{q}} \hat{\mathbf{b}}\cdot\mathbf{k}\times\mathbf{q}\, n_{\mathbf{q}}\phi_{\mathbf{k}-\mathbf{q}}, \tag{3}$$

where $\bar{\nu} = (m_e/m_i)(\nu_e^2 + \Omega_e^2)/\nu_e$, $\mathbf{V}_{de0}$ is the zero-order electron drift (primarily an $\mathbf{E} \times \mathbf{B}$ drift), $\hat{\mathbf{b}}$ is a unit vector in the direction of $\mathbf{B}_0$, and the sum on $\mathbf{q}$ is a sum over available spatial Fourier modes characterized by wavenumber $\mathbf{q}$. In this expression, all nonlinear terms have been discarded except for the electron $\mathbf{E} \times \mathbf{B}$ term, which appears on the right-hand side.

[1]Currently at the Department of Biomedical Engineering, Case Western Reserve University, Cleveland, OH 44106.

Paper number 98GL50868.
0094-8534/98/98GL-50868$05.00.

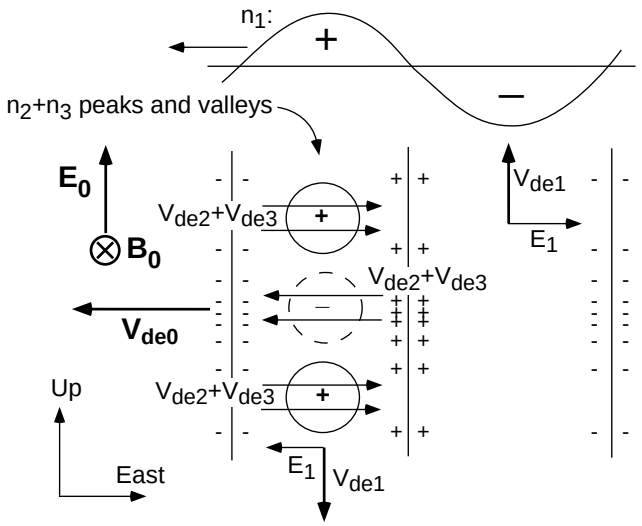

Figure 1. Sketch of the saturation mechanism.

To study the saturation mechanism, we solved Eqs. (1–3) numerically, keeping only three spatial Fourier modes: mode 1, which represents the primary linearly-unstable Farley-Buneman wave traveling horizontally West with wavevector $\mathbf{k}_1$, and modes 2 and 3, which travel vertically and obliquely, respectively, with wavenumbers $\mathbf{k}_2$ and $\mathbf{k}_3$, to represent the vertically propagating secondary wave. The purpose of this restricted model is to provide insight into the nonlinear saturated state; thus, the model should not be expected to accurately represent the full detailed behavior of the instability. We somewhat arbitrarily chose $\mathbf{k}_2$ pointing downward, to study downward propagating secondary modes on the primary mode density crests. Each spatial Fourier mode is composed of the Fourier coefficients $n_{\mathbf{k}}$, $\mathbf{u}_{i\mathbf{k}}$, and $\phi_{\mathbf{k}}$, for the various dynamic perturbed quantities, together with the set of coefficients $n_{-\mathbf{k}}$, $\mathbf{u}_{i(-\mathbf{k})}$, and $\phi_{-\mathbf{k}}$, which are related to the first set through the reality conditions $n_{-\mathbf{k}} = n^*_{\mathbf{k}}$, etc. Two modes are required to model the secondary wave in order to constrain its density variations to lie on the primary wave's density peaks, as observed in the particle simulation. This constraint also requires $\mathbf{k}_3$ to satisfy $\mathbf{k}_1 + \mathbf{k}_2 + \mathbf{k}_3 = 0$ once $\mathbf{k}_1$ and $\mathbf{k}_2$ are chosen, which is also the condition needed for three-wave mode coupling.

Results from the Model

When the model with $\mathbf{k}_1 = -2\hat{\mathbf{x}}\ \mathrm{m}^{-1}$ and $\mathbf{k}_2 = -5\hat{\mathbf{z}}\ \mathrm{m}^{-1}$, and parameters typical of the topside daytime equatorial E-region ($\mathbf{E}_0 = 14\hat{\mathbf{z}}$ mV/m, $n_0 = 2\times10^{11}$ m^{-3}, $\nu_e = 1.7\times10^4$ sec^{-1}, $\nu_i = 950$ sec^{-1}, $B_0 = 0.25$ gauss, ion mass m_i of 5.01×10^{-26} kg, and $(\gamma_i T_i)^{1/2}/m_i = (\gamma_e T_e/m_i)^{1/2} = 265$ m/s, implying a zero-order drift speed of 560 m/s and a sound speed of 375 m/s) was initialized with density perturbations, $n_1 = n_2 = n_3 = 0.005n_0$, the principal wave density n_1 initially grew exponentially with the expected linear growth rate and frequency, while the other modes linearly decayed. When the nonlinear $\mathbf{E}\times\mathbf{B}$ term started to become important, the amplitudes of the secondary modes n_2 and n_3 grew rapidly while n_1 saturated. For many of the parameters we examined (but not all), the system eventually arrived at a stationary state, with n_1, n_2, and n_3 maintaining constant amplitudes and oscillating sinusoidally with frequencies ω_1, ω_2, and ω_3 satisfying $\omega_1 + \omega_2 + \omega_3 = 0$.

The saturated state densities, phases, and frequencies were found to match exactly those obtained from a nonlinear dispersion relation solver we constructed using time-Fourier transformed versions of Eqs. (1–3). The mode phase velocities were reduced significantly from the linear phase velocity (535 m/s) to values around the sound speed (375 m/s) in rough agreement with the particle simulation and observations. Specifically, we obtained mode phase velocities of $|\omega_1/k_1| = 0.83C_s$, $|\omega_2/k_2| = 0.95C_s$, and $|\omega_3/k_3| = 1.19C_s$ in the ion frame. These numbers suggest that the independence of phase velocity on the propagation direction elevation angle θ seen in observations, which is at odds with the $\cos\theta$ dependence predicted by linear theory, *is* consistent with the three-mode coupling mechanism we use in our model. The saturated perturbed densities, $|n_1| = 0.075n_0$, $|n_2| = 0.050n_0$, and $|n_3| = 0.035n_0$, were slightly higher than those typically observed (about 5% for the total density fluctuation) and those seen in particle simulations (an rms value of 2.7% in the simulations described below). The qualitative discrepancy may be due to the inability of the energy in these three modes to couple to other modes, as would be the case in the simulation or in the electrojet.

The Saturation Mechanism

The saturation mechanism leading to this stationary state may now be described in simple terms. In the dayside equatorial electrojet, the zero-order electric field $\mathbf{E}_0$ usually points almost straight up, which produces an electron $\mathbf{E}\times\mathbf{B}$ drift to the west, shown as $\mathbf{V}_{de0}$ in Fig. 1. When the drift exceeds the linear stability criterion, a primary Farley-Buneman wave begins to grow and propagate west. Within the wave, the electrons in the wave density peaks are carried ahead (westward) of the ions by the zero-order electron drift, $\mathbf{V}_{de0}$. This charges the leading edge (the westward edge) of the primary wave density wavefronts negative, as indicated by the columns of minus signs in Fig. 1. The trailing edges are correspondingly charged positive. These charges set up the primary wave electric field, $\mathbf{E}_1$, which points in the direction of $\mathbf{V}_{de0}$ in the primary wave density peaks, and antiparallel to $\mathbf{V}_{de0}$ in the density valleys.

The electric fields $\mathbf{E}_1$ then drive electron $\mathbf{E}\times\mathbf{B}$ drifts of their own. The drifts, $\mathbf{V}_{de1}$, are downward along the density crests of the primary wave, and upward in the valleys. Eventually, the primary wave, and therefore $\mathbf{V}_{de1}$, grow to amplitudes large enough to drive a secondary Farley-Buneman wave downward along the primary wave density crests. (Upward propagating secondary waves traveling in the primary wave density valleys, which are seen in the particle simulation, are inhibited from appearing here, because there is no upward, westward-pointing $\mathbf{k}$ in the system to represent them.) In analogy to the primary wave, the secondary wave density peaks and valleys are accompanied by secondary wave electric fields which roughly point, respectively, parallel and anti-parallel to the driving $\mathbf{E}\times\mathbf{B}$ drift, $\mathbf{V}_{de1}$. These secondary electric fields, in turn, set up secondary $\mathbf{E}\times\mathbf{B}$ electron drifts, shown in Fig. 1 as $\mathbf{V}_{de2} + \mathbf{V}_{de3}$.

The key to the saturation of the primary wave lies in how these secondary $\mathbf{E}\times\mathbf{B}$ drifts modify the charge buildup on the leading edge of the primary wave. In the secondary wave density depletion region, indicated by the dashed circle la-

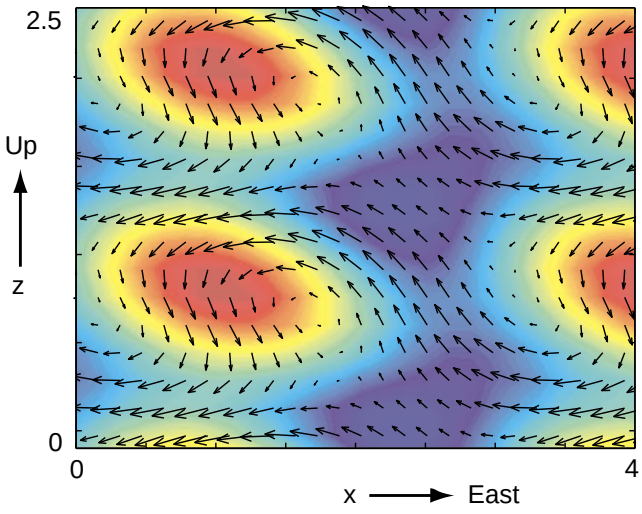

Figure 2. Color plot of the total density and vector plot of the $\mathbf{E} \times \mathbf{B}$ flow field obtained from the reduced-mode computer model during stationary state behavior. Red represents the regions of highest density, blue, the lowest density.

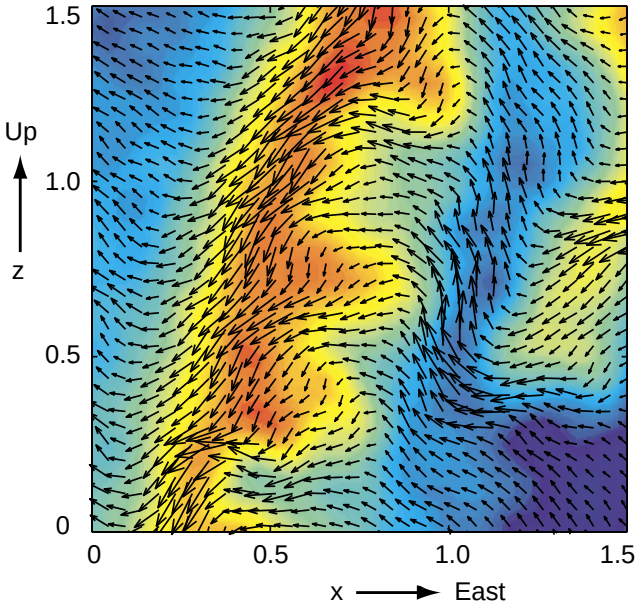

Figure 3. Color plot of the total density and vector plot of the $\mathbf{E} \times \mathbf{B}$ flow field obtained from the particle simulation. Red represents the regions of highest density, blue, the lowest density.

beled with a minus sign in Fig. 1, the secondary drift is in the same direction as $\mathbf{V}_{de0}$, but is pushing forward less electrons, because it is operating in a density depletion. Meanwhile, in the secondary density enhancement regions (circles labeled with pluses), there are more electrons available, but they are being pushed by $\mathbf{V}_{de2} + \mathbf{V}_{de3}$ against the zero-order flow to the *trailing* edge of the primary wave, thereby partially canceling the primary wave charge buildup. Both processes thus reduce the charging effect produced by $\mathbf{V}_{de0}$ for the primary wave. Since $\mathbf{V}_{de0}$ drives the primary wave instability, the tendency of the secondary wave to reduce its effect is stabilizing. In other words, the mean transport of electrons by the secondary wave via its $\mathbf{E} \times \mathbf{B}$ drift is in a direction opposite that of $\mathbf{V}_{de0}$, which therefore partially cancels the latter's destabilizing effect.

A slightly different interpretation of the stability mechanism arises from an examination of the stationary state viewed as a whole. Figure 2 shows the total electron $\mathbf{E} \times \mathbf{B}$ flow field (including $\mathbf{V}_{de0}$) superimposed on the total charge density. We see that the zero-order electron flow $\mathbf{V}_{de0}$, is almost completely cancelled by $\mathbf{V}_{de2} + \mathbf{V}_{de3}$ in the secondary wave density enhancement regions, leaving only the downward directed $\mathbf{V}_{de1}$ flow. The zero-order flow is thus largely unable to take advantage of these density enhancements to produce charge buildup for the primary wave. In the secondary wave density depletion regions, located between the enhancement regions vertically, there is substantial east-to-west flow, but only a slight density gradient to work with. Again, this diminishes the flow field's ability to build charge. In short, the secondary wave is saturating the primary wave by shuttling the zero-order electron drift around the density peaks through the action of its own $\mathbf{E} \times \mathbf{B}$ flow field. With most of the flow in regions of flatter density, less charge is accumulated on the primary wave wavefronts, and the wave is stabilized.

This saturation mechanism also appears to play a dominant role in the saturation of the Farley-Buneman instability in our particle simulations. These simulations employ a particle-in-cell technique to model fully kinetic ion behavior, while the electrons behave as an inertialess fluid, as described in [*Oppenheim et al.*, 1995, 1996]. Figure 3 shows the density and $\mathbf{E} \times \mathbf{B}$ flow field from the particle simulation well after its saturation point. As in the mode-coupling model, the strongest westerly electron flow along the primary peak density wavefront occurs in the secondary wave density valleys (at locations $(x, z) = (0.37, 0.25)$, (0.42,0.60) and (0.58,1.12) in Fig. 3). There is also a noticeably more westerly flow at $(x, z) = (0.52, 0.95)$. Otherwise, the electron flow is directed roughly along the length of the wavefront, as expected (cf. Fig. 2). These effects vanish when we disable the nonlinear electron $\mathbf{E} \times \mathbf{B}$ response in the simulation. In this case, the instability saturates at a much higher level through ion trapping. We conclude that, while other processes are at work in the simulation, producing features such as the tilted orientation and more complicated structure of the primary wavefront evident in Fig. 3, our mode-coupling mechanism is clearly present and is likely responsible for the saturation of the primary Farley-Buneman wave.

Summary and Comparison to Other Theories

A saturation mechanism for the Farley-Buneman instability has been described which operates by reducing the charge separation generated by the zero-order $\mathbf{E} \times \mathbf{B}$ electron drift, the driving force for this instability. The reduction in charge comes about through a reorganization of the zero-order drift around local density peaks orchestrated by secondary waves propagating along the primary Farley-Buneman wavefronts. The secondary waves are driven by the primary wave's $\mathbf{E} \times \mathbf{B}$ drifts in manner similar to that described originally by *Sudan et al.* [1973] for gradient-drift waves. The present model differs from Sudan *et al.*'s, however, in that the local approximation is not valid here, since

the primary and secondary wave wavelengths are comparable, and so must be replaced by a more complicated mode-coupling model which involves both obliquely and vertically propagating modes. These secondary modes produce a net electron flux across each primary wavefront in a manner similar to that described by *Kudeki et al.* [1985], except that the flux here is horizontal rather than vertical, is being generated by secondary waves rather than the primary wave, and again, requires a mode coupling model. It is this flux which acts to reduce the primary wave charge separation. Mathematically, our model is more strongly coupled than the one described by *Sahr and Farley* [1995], which was aimed primarily at type-3 and type-4 irregularities. In particular, we allow for nonlinear frequency shifts for the various modes. In this respect, our model resembles that of *Hamza and St-Maurice* [1993], and in fact is a special case of the mathematical groundwork presented therein. Our model apparently diverges from *Hamza and St-Maurice* [1993], however, on its wave statistical assumptions. The details of this comparison, together with further characteristics of the saturated state derived from our reduced-mode models, will be presented in future communications.

References

Buneman, O., Excitation of field aligned sound waves by electron streams, *Phys. Rev. Lett.*, *10*, 285, 1963.

Farley, D. T., A plasma instability resulting in field-aligned irregularities in the ionosphere, *J. Geophys. Res.*, *68*, 6083, 1963.

Hamza, A. M., and J.-P. St-Maurice, A turbulent theoretical framework for the study of current-driven E region irregularities at high latitudes: basic derivation and application to gradient-free situations, *J. Geophys. Res.*, *98*, 11587–11599, 1993.

Kudeki, E., D. T. Farley, and B. G. Fejer, Theory of spectral asymmetries and nonlinear currents in the equatorial electrojet, *J. Geophys. Res.*, *90*, 429–436, 1985.

Oppenheim, M., and N. Otani, Spectral characteristics of the Farley-Buneman instability: simulations versus observations, *J. Geophys. Res.*, *101*, 24572–24582, 1996.

Oppenheim, M., N. Otani, and C. Ronchi, Hybrid simulations of the saturated Farley-Buneman instability in the ionosphere, *Geophys. Res. Letters*, *22*, 353–356, 1995.

Oppenheim, M., N. Otani, and C. Ronchi, Saturation of the Farley-Buneman instability via nonlinear electron ExB drifts, *J. Geophys. Res.*, *101*, 17273–17286, 1996.

Sahr, J. D., and D. T. Farley, Three-wave coupling in the auroral E-region, *Ann. Geophysicae*, *13*, 38–44, 1995.

Sudan, R. N., Unified theory of type I and type II irregularities in the equatorial electrojet, *J. Geophys. Res.*, *88*, 4853–4860, 1983.

Sudan, R. N., J. Akimrimisi, and D. T. Farley, Generation of small-scale irregularities in the equatorial electrojet, *J. Geophys. Res.*, *78*, 240–248, 1973.

N. F. Otani, Department of Biomedical Engineering, Wickenden Building, Case Western Reserve University, Cleveland, OH 44106. (e-mail: otani@reentry.ebme.cwru.edu)

M. Oppenheim, Physics Department, CB 390, University of Colorado, Boulder, CO 80309. (e-mail: meers@electrojet.colorado.edu)

(Received December 14, 1997; accepted February 3, 1998.)